WILEY-VCH

Title: Reversible and irreversible reactions of trimethylaluminium with common organic functional groups as a model for molecular layer deposition and vapor phase infiltration

Fan Yang, Jens Brede, Hayrensa Ablat, Mikel Abadia, Lianbing Zhang, Celia Rogero, Simon D. Elliott, Mato Knez[*]

Dr. Fan Yang, Prof. Dr. Mato Knez
CIC nanoGUNE Consolider, Tolosa Hiribidea 76, 20018 Donostia-San Sebastian, Spain
E-mail: m.knez@nanogune.eu
Dr. Jens Brede, Mikel Abadia, Dr. Celia Rogero
Centro de Física de Materials, Paseo Manuel de Lardizabal, 5, 20018 Donostia-San Sebastian, Spain
Hayrensa Ablat, Dr. Simon D. Elliott
Tyndall National Institute, University College Cork, Lee Maltings, Dyke Parade, Cork, T12 R5CP, Ireland
Dr. Lianbing Zhang
School of Life Sciences, Northwestern Polytechnical University, 710072 Xi'an, China
Dr. Celia Rogero,
Donostia International Physics Center (DIPC), Paseo Manuel de Lardizabal, 4, 20018 Donostia-San Sebastian, Spain
Prof. Dr. Mato Knez,
IKERBASQUE, Basque Foundation for Science, Maria Diaz de Haro 3, 48013 Bilbao, Spain

Abstract: Organic-inorganic hybrid materials are of great demand not at least for their enormous application potential in flexible devices. Atomic or molecular layer deposition (ALD or MLD) and vapor phase infiltration (VPI) offer novel pathways for the fabrication of such hybrids, but a clear understanding of the chemistry between the vaporized precursors and functional molecules is still lacking. In this work, we investigate the interactions between trimethylaluminum (TMA) and the organic functional groups –OH, –NH$_2$ and –NO$_2$ in the respective substituted phenyls, as well as their stability upon exposure to air. The experimental evidence agrees with theoretically predicted reaction pathways, showing that TMA initially binds to Lewis basic atoms of the investigated functional groups. Depending on the reaction energy barriers, the interaction between TMA and the investigated functional groups may result in either stable chemical bonding or intermediates that decompose upon exposure to humidity. This investigation

contributes to the understanding of ALD/MLD and VPI processes at a molecular level and will support a better process optimization.

Introduction

Organic-inorganic hybrid materials are very attractive, promising a beneficial combination of the advantages of both organic and inorganic material worlds. Often they bring about novel aspects for practical applications[1], like biocompatible artificial organs or engineered tissues[2–4]. Atomic layer deposition (ALD) is an innovative approach towards producing such hybrid materials. It has been refined in two specific ways: molecular layer deposition (MLD)[5–7] for thin film growth and vapor phase infiltration (VPI)[8] for modification of soft matter in the subsurface area.

The MLD process closely resembles the ALD process with vaporized reactive precursors being separately introduced into a reactor where they *react* with the substrate surface. The difference of MLD to ALD mainly refers to the choice of precursors, in MLD at least one of the precursors being substituted with an organic molecule. This strategy has proven to be very versatile, so that zincones[9–13], alucones[14–16], titanicones[17–19] and many other hybrid materials [20,21] have been successfully grown by MLD. The resulting deposited hybrid coatings often exhibit interesting chemical or physical properties, which are distinct from those of their corresponding metal oxides and polymers.
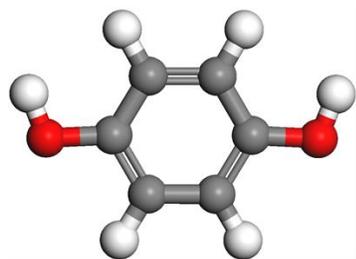
Vapor phase infiltration (VPI) is another way to fabricate organic-inorganic hybrid materials using the ALD processing technology. In an infiltration process, typical metal organic ALD precursors are pulsed into the reactor and, instead of saturating the surface of a substrate, which is usually a natural or synthetic polymer, they are allowed to *diffuse into* its subsurface area. This is achieved with an extended exposure time, during which the precursor penetrates the bulk and interacts with the embedded functional organic groups[22–27]. VPI has been used in several variations for designing and synthesizing new hybrid materials ranging from technical polymers to individual molecules. A prominent example for the latter case is the metalation of porphyrins with Zn upon infiltration of J-aggregates with diethylzinc (DEZ)[22]. On a larger scale, it has been shown that the strength and toughness of the spider dragline silk have been greatly enhanced after such infiltration[24].

WILEY-VCH

Both MLD and VPI have been broadly studied and show great potential for hybrid material synthesis and soft material modification. However, the mechanisms of the chemical reactions between the metal precursors and the organic functional groups in either MLD or VPI are not understood in detail. The processing strategies rely on trial-and-error experiments and chemical intuition. The latter is mainly derived from the present knowledge in organic and metal-organic reactivity in solvent-based chemistry, and may therefore not necessarily reflect the reactivity in absence of solvents and at low pressure, which are typical conditions for both MLD and VPI[28].

With this in mind, we performed fundamental investigations on the reactivity between the most common ALD precursor trimethylaluminium (TMA) and a selection of organic molecules with very different chemical character, as shown in Figure 1. We used benzene rings functionalized with amine, nitro or hydroxyl groups, since those functionalities are common for many polymers. Thus, the molecules used in this work represent various classes of organic molecules, oligomers or polymers involved in MLD or VPI processes.

Density functional theory (DFT) is a powerful tool to investigate mechanisms of chemical reactions and hence predict the most suitable precursors and process conditions [28,29]. However, only few DFT studies have addressed aspects of MLD experiments so far [29–31]. In our approach, we evaluate the reaction mechanisms between the bespoke molecules and TMA and the stabilities of the intermediates in a concerted way by using DFT and semi *in-situ* XPS experiments. We find that the height of the energy barrier that needs to be overcome for strengthening the chemical bonding between TMA and the various functional groups is a crucial factor for a reaction. Upon initial binding of TMA to the respective functional group, the activation energy for dissociation of the methyl ligand from Al determines whether the reaction sequence will proceed or reverse. We find that this is strongly dependent on the functional group. This investigation is a step towards understanding and controlling the MLD and VPI processes at the molecular level, which will certainly be helpful for the optimization of hybrid material fabrication in future.
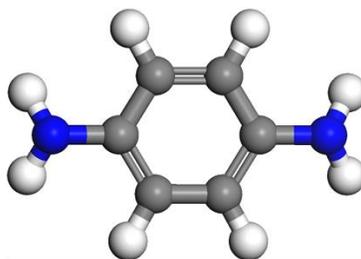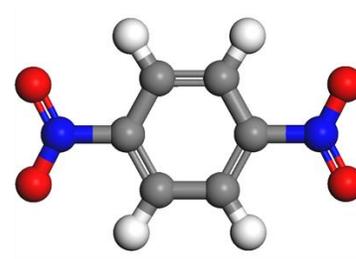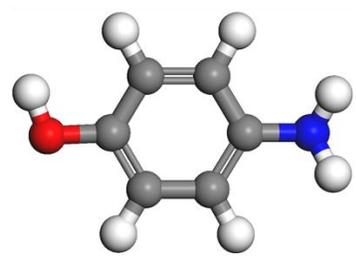
WILEY-VCH

4-hydroquinone (4HQ)

4-phenylenendiamine (4PD)

4-dinitrobenzene (4DN)

4-aminophenol (4AP)

4-nitroaniline (4NA)

4-nitrophenol (4NP)

trimethylaluminum (TMA)

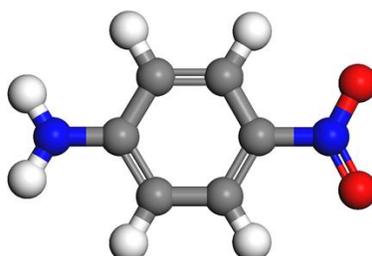| H | O | N | C | Al |

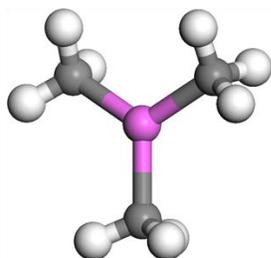**Figure 1** Structures of 4-hydroquinone (4HQ), 4-phenylenediamine (4PD), 4-dinitrobenzene (4DN), 4-aminophenol (4AP), 4-nitroaniline (4NA), 4-nitrophenol (4NP), and trimethylaluminium (TMA) after optimization by DFT.

Experimental section

A set of di-substituted phenyls with all possible homogenous and heterogeneous combinations of hydroxyl, amino and nitro groups were chosen as substrates for the experiments, including 4-hydroquinone, 4-phenylenediamine, 4-dinitrobenzene, 4-nitrophenol, 4-aminophenol and 4-nitroaniline (Figure 1). All molecules were purchased from Sigma-Aldrich. The chemicals were of analytic grade and were used as received unless otherwise stated.

Semi-in-situ MLD/XPS experiments. In order to avoid contamination from air and humidity, exposure of the substrates to TMA was also performed inside of a load-lock that was connected with the ultrahigh vacuum (UHV) chamber of an XPS. For this purpose, the substrate chemicals were pressed into pellets and mounted onto molybdenum sample plates with commercial carbon tape. Although care was taken to completely cover the carbon tape with the pellets, some contribution from the carbon tape to the resulting XPS spectra cannot be excluded. The samples were introduced into the load-lock of the UHV system. After evacuating the load-lock to about 10^{-6} mbar the pellets were transferred into the UHV-XPS chamber operating at a base pressure of 3×10^{-10} mbar. The samples were cooled down to about 100 K to prevent sublimation and measured. After the reference measurements, the samples were transferred back into the load-lock and allowed to heat up to room temperature. Then the pellets were exposed to TMA by introducing the vapors directly into the load-lock, maintaining a TMA partial pressure of several mbar for several tens of seconds. Subsequently, the load-lock was re-evacuated and the samples were transferred back into the UHV chamber, cooled down and measured with XPS. Finally, the samples were transferred back again into the load-lock to test the stability of the bonding between TMA and the molecules by venting the load-lock and exposing the sample to air. After exposure, the load-lock was evacuated again, and the sample was transferred back into the XPS/UHV chamber and measured. Thus, each sample was measured three times: prior to TMA dosing, after TMA dosing and after exposure to air.

As MLD processes are performed on solid substrates, an MLD type of growth using TMA and 4-phenylenediamine as precursors on a highly reduced single crystalline TiO_2 (110) substrate was also investigated in the load-lock. The TiO_2 surface is well characterized and therefore suitable for characterization by XPS, while at the same time it is representative of numerous typically used metal oxide based substrates. In this process, TMA was initially dosed with a partial pressure of $p_{TMA} > 10^{-3}$ mbar for several tens of seconds in order to bind to the hydroxylated TiO_2 surface. Subsequently, the ALD reactor was evacuated to a pressure below 10^{-4} mbar and the sample was rapidly transferred into the UHV chamber. The XPS measurements were performed under UHV conditions ($p < 10^{-9}$ mbar) at room temperature. In the next stage, the sample was transferred back into the molecule deposition chamber (base pressure below 10^{-8} mbar) and dosed with several thousands of Langmuir of 4-phenylenediamine to ensure saturative coverage. Subsequently, the sample was transferred again into the XPS

chamber and measured. The stability of the interaction between 4-phenylenediamine and TMA was finally tested by dosing H_2O into the reactor and measured again in the UHV chamber. The reverse dosing sequence with first 4-phenylenediamine, second TMA and finally with H_2O was also tested. Therefore, each TiO_2 sample was measured four times: clean TiO_2 surface, after TMA (or 4-phenylenediamine) dosing, after 4-phenylenediamine (or TMA) dosing and finally after water dosing.

The XPS experiments were performed using a Phoibos photoelectron spectrometer equipped with an Al Kα X-ray source as the incident photon radiation. While the incident photon radiation is fixed, complications arise due to charging effects during measurements of the pellet samples. The C 1s core levels of the phenyl ring between 285.0 and 287.0 eV were used for calibration based on earlier reported data[32–40]. Specifically, the signal at 285.0 eV was assigned to the four non-functionalized carbon atoms in the central part of the phenyl ring, while the peaks at 286.3 eV, 286.1 eV and 286.7 eV were assigned to the carbon atoms bound to amine, nitro and hydroxyl groups, respectively (see supporting information). The carbon tape may contribute to the signal intensity in the region 286.0-287.0 eV. However, the contribution is minor, and may merely change the peak intensity ratio of the four central carbon atoms of the phenyl ring to the two functionalized carbon atoms (2:1 in the ideal case). All N, Al and O spectra were calibrated and normalized according to the position and intensity of the C 1s core level. For the surface samples, the Ti 2p peak was used for the binding energy calibration. The overall resolution of the instrument is approximately 0.9 eV. At this resolution, the line energy positions could be determined with an accuracy of ±0.2 eV.

Computational Method. All DFT calculations were carried out with the Perdew–Burke–Ernzerhof (PBE) exchange-correlation density functional[41] and the SV(P) basis set (double zeta valence basis set with polarization at all non-hydrogen atoms) with the resolution of density (RI) approximation for Coulomb integrals[42] accompanied by the corresponding auxiliary basis sets[43] as implemented in TURBOMOLE[44]. Geometries were freely optimized using redundant internal coordinates[45] until gradients were $< 10^{-3}$ Hartree/Bohr. Optimized structures were visualized with Materials Studio suite version 7.0.

Results and Discussion

Reactivity of TMA with homo-substituted phenyl molecules

The interactions between TMA and the three functional groups hydroxyl, amine and nitro were experimentally studied with XPS by tracing the changes of the C 1s, N 1s, O 1s, Al 2s and Al 2p core levels. Specifically, we measured the pristine 4HQ, 4PD and 4DN molecules before and after exposure to TMA and finally after exposure to air. In this way contamination by the environment was minimized and even metastable states could be identified. By applying X-rays with a low intensity, beam damage was minimized; indeed, only the nitro group showed some indications of X-ray induced reduction and cleavage, which is known from literature[34,46].

Figure 2 shows the C 1s, N 1s and Al 2p XPS spectra of the three molecules. In Figure 2a, the C 1s core levels of pristine 4HQ, 4DN and 4PD are shown. The line shapes of the core levels of the three samples are symmetric but rather broad with a full width of half maximum (FWHM) being larger than 2.5 eV. This width stems from the contribution of two chemically non-equivalent carbon species within the phenyl ring, the four H-substituted and two functionalized carbon atoms. The H-substituted carbon atoms were assigned to 285 eV, while the functionalized carbon atoms were assigned to 286.7 eV (C-OH), 286.3 eV (C-NH$_2$) and 286.1 eV (C-NO$_2$), respectively[32–40].

All changes of the C 1s, N 1s and Al 2s signals after the various exposures are summarized in Table S1. As can be seen in Figure 2a, upon exposure of 4HQ to TMA and subsequently to air, the C 1s shows only marginal changes. In contrast, the C 1s peaks of 4PD and 4DN become asymmetric after TMA dosing, indicating a new contribution at lower binding energies (BEs) of ~283.5 eV. The contribution can be assigned to the –CH$_3$ from TMA, albeit substantially lower than the 284.8 eV reported by Lubben[47] and Strongin[48] for condensed TMA films. Subsequent exposure to air results in a significant loss of those contributions, but neither of the samples fully recovers the pristine state.

Figure 2b shows the Al 2p core level spectra of the same samples. Pristine samples did not contain Al and were therefore featureless and are consequently not shown. After TMA dosing, the main feature of the Al 2p core level of the 4HQ sample developed at 75.7 eV, while the 4 PD and 4DN samples had their main features at 73.6 eV and 73.8 eV, respectively. After subsequent exposure to air, the Al 2p core level peaks of 4HQ remained nearly unchanged, while those of 4PD and 4DN shifted noticeably towards higher binding energies.
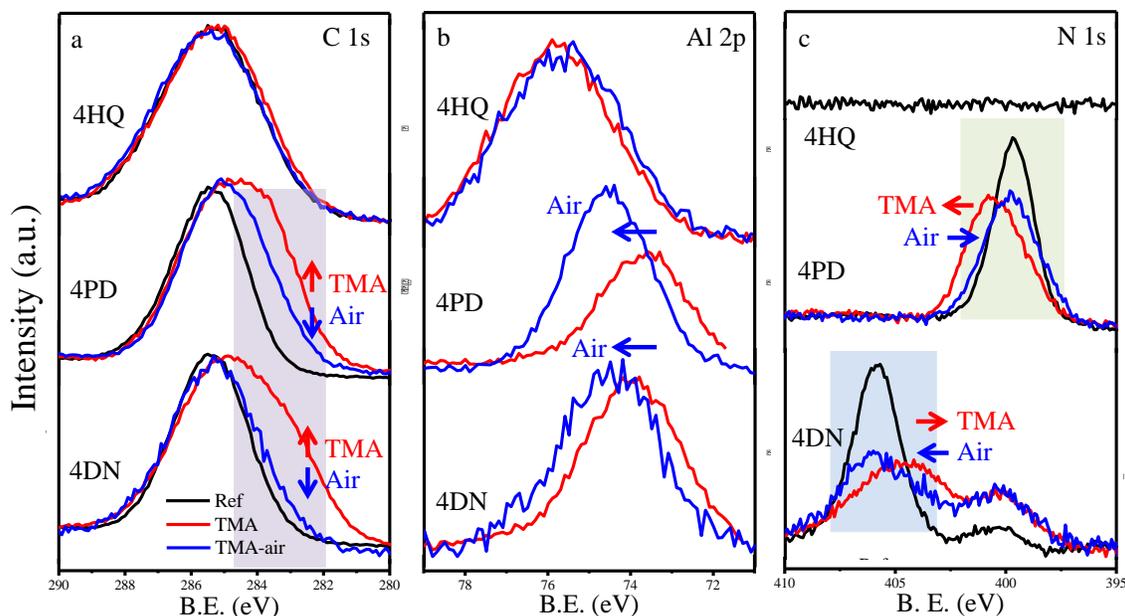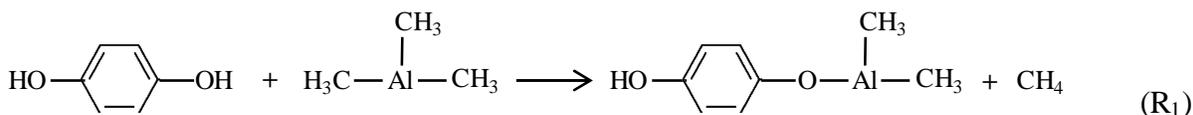
Figure 2. (a) C 1s, (b) Al 2p and (c) N 1s spectra of 4-hydroquinone (4HQ), 4-dinitrobenzene (4DN) and 4-phenylenediamine (4PD) in the native (black curve), TMA dosed (red curve) and air exposed (blue curve) states. Arrows in the figures indicate the changes of the peaks in the marked zone upon exposure to TMA and subsequently to air.

The N 1s core level spectra of the samples are shown in Figure 2c. Since 4HQ does not contain nitrogen, no signal is observed. The 4PD sample shows a single peak at 399.6 eV, which can be assigned to the amine group (–NH$_2$)[33] in the pristine sample. After TMA dosing the peak becomes asymmetric with a dominating component at Binding Energies (BEs) higher than 400 eV. Upon subsequent exposure to air, the peak recovers its position (BE=399.6 eV), but becomes broader. The pristine 4DN sample shows two peaks in the N 1s region. The peak centered around 406 eV corresponds to the NO$_2$ group, which is in good agreement with the literature[32,34,49]. The second and less intense feature located around 400 eV indicates a partial X-ray induced reduction of nitro groups to amine groups[34] or selective cleavage[46]. After dosing with TMA, the NO$_2$ peak shifts towards lower binding energies (405 eV), while the 400 eV feature remains largely unaffected. After subsequent exposure to air, only the peak at higher BE shifts back to around 406 eV, while the peak at around 400 eV remains unchanged.

The XPS spectra show that in dependence on the chosen functional group either stable reaction products or metastable intermediates can occur. Especially the nature and quality of the intermediates may be difficult to identify by the XPS spectra only. For better interpretation of the

mechanisms, we performed DFT calculations for a reaction of the precursor with the three homo-substituted phenyls. The modeling was done via transition state search for the binding of TMA, potential proton transfer and elimination of CH_4. Since the proximity of neighbouring molecules in MLD films is difficult to judge, only intramolecular proton transfer was considered. We further considered that the by-product CH_4 might form repeatedly if sufficient protons and methyl groups are available at the reaction sites. Finally, we considered possible subsequent reactions with water as an indicator for the stability of the reaction product upon exposure to humidity. This appears to be one of the major problems of MLD deposited thin films.

The Al atom in TMA is sp^2 hybridized, where one 3s and two 3p occupied orbitals bind to three methyl groups[50–53]. The remaining empty 3p orbital defines its strong Lewis acidity and contributes to the high reactivity of TMA towards adsorption in ALD processes. The –OH groups in 4HQ have lone electron pairs of Lewis basic character, as well as Brønsted acidic protons that can bind with the methyl ligands and eliminate as CH_4. Therefore, the initial reaction between 4HQ and TMA is likely to be as follows:

$$HO\text{---}\langle\bigcirc\rangle\text{---}OH \ + \ H_3C\text{---}\underset{\underset{CH_3}{|}}{Al}\text{---}CH_3 \longrightarrow HO\text{---}\langle\bigcirc\rangle\text{---}O\text{---}\underset{\underset{CH_3}{|}}{Al}\text{---}CH_3 \ + \ CH_4 \qquad (R_1)$$

We determined the energetic profile of the reaction R_1 by geometry optimization and transition state search using DFT. The resulting model predicts a two-step process for the reaction, where initially the empty 3p orbital of Al in TMA overlaps with the lone electron pair of the O in 4HQ, and forms a Lewis adduct. This corresponds to the E_2 state in Figure 3. The calculated activation energy is negligible (E_1-E_0=3.1 kJ/mol) and thus the reaction is considered to be spontaneous. Thereafter, one of the methyl groups of TMA would react with the H atom from the –OH group forming CH_4. The energy barrier for this intramolecular proton transfer is only E_3-E_2=32.5 kJ/mol and lower than comparable barriers calculated for the formation of alumina by ALD[50–52]. The newly formed CH_4 desorbs without a barrier, leaving dimethylaluminium chemically bound to the hydroxyphenoxide molecule (E_4 in Figure 3 错误!未找到引用源。). The overall energy gain for R_1 is calculated to be ΔE=-149.7 kJ/mol.

It is worth noting that further 4HQ molecules may react with the two remaining methyl groups of TMA. The possible scenarios are shown in Figure 4. The energy gains after further eliminations of CH_4 amount to -154.6 kJ/mol for R_{1-1} relative to the E_4 state in Figure 3 and -

140.9 kJ/mol for R_{1-2} relative to R_{1-1}. In view of those values, all those reactions are likely to happen. Indeed, the C 1s and Al 2p core level peaks of 4HQ in Figure 2b remain the same before and after exposure to air, indicating a quantitative reaction of TMA with 4HQ that consumes all available methyl groups.
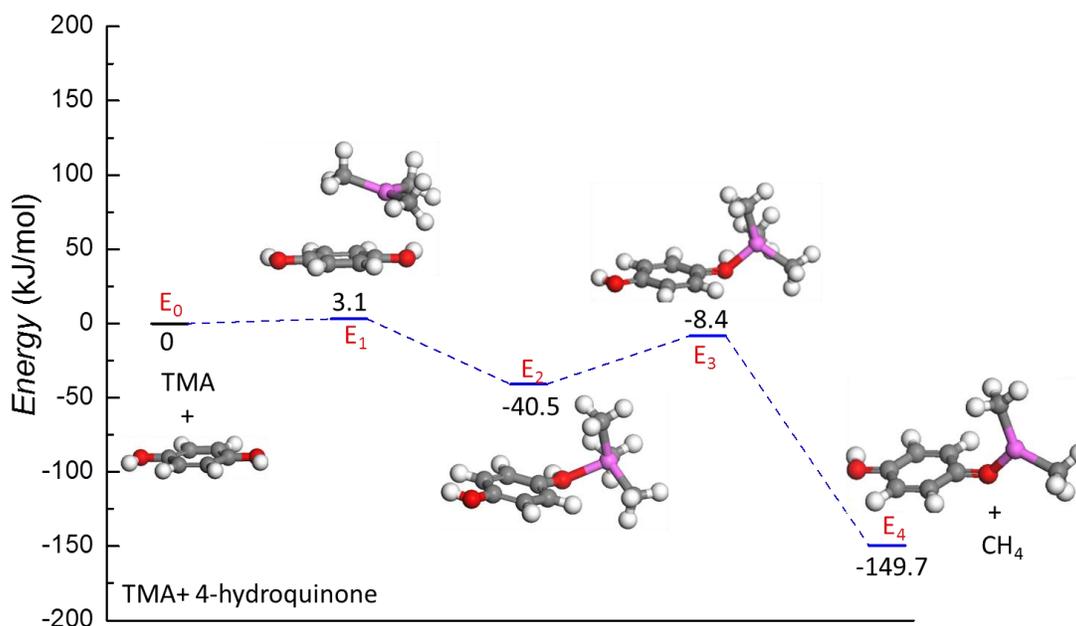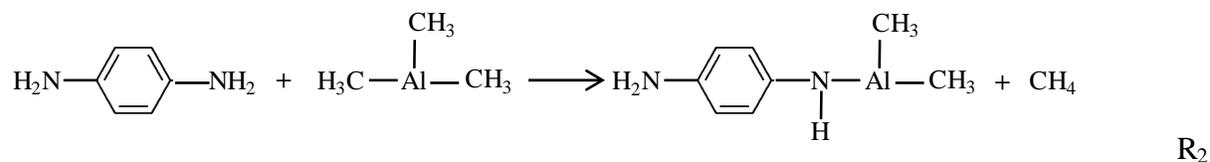

Figure 3. Calculated energy profile for the reaction pathway R_1 of TMA interacting with 4HQ.


R_{1-1} (-154.6 kJ/mol) R_{1-2} (-140.9 kJ/mol)
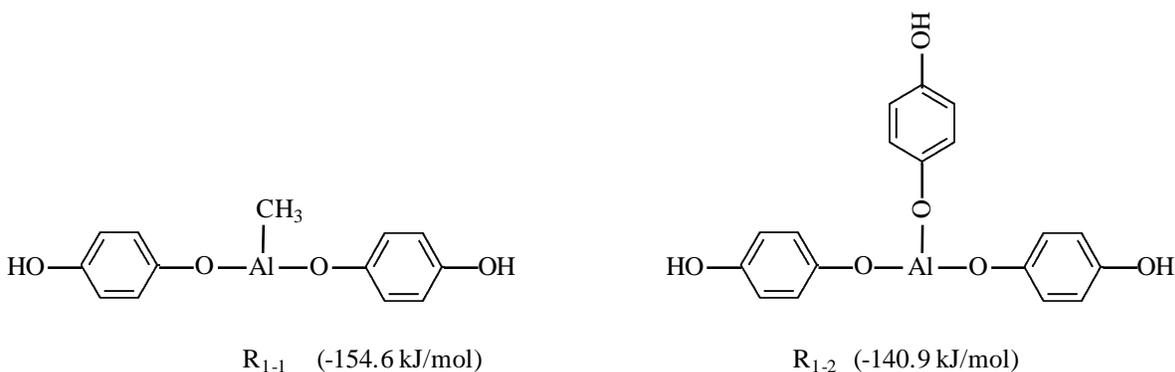
Figure 4. Possible products after reactions of a single TMA with multiple 4HQ molecules. Energy gains after elimination of CH_4 are -154.6 kJ/mol for R_{1-1} relative to E_4 (Figure 3) and -140.9 kJ/mol for R_{1-2} relative to R_{1-1}.

In a similar way, the chemical reaction between 4PD and TMA was also calculated according to the following reaction scheme:

$$H_2N-\bigodot-NH_2 \;+\; H_3C-\underset{\underset{CH_3}{|}}{Al}-CH_3 \longrightarrow H_2N-\bigodot-\underset{\underset{H}{|}}{N}-\underset{\overset{|}{CH_3}}{Al}-CH_3 \;+\; CH_4$$

$$R_2$$

The reaction may proceed further according to the following scheme:

$$H_2N-\bigodot-\underset{\underset{H}{|}}{N}-\underset{\overset{|}{CH_3}}{Al}-CH_3 \longrightarrow H_2N-\bigodot-N=Al-CH_3 + CH_4$$

$$R_2{}^*$$
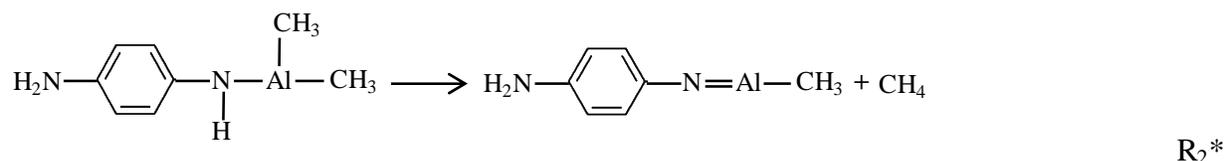
The energy profile for the reactions R_2 and R_2* is shown in Figure 5**Figure** . Similar to the previous case, –NH_2 also contains a lone electron pair and is a Lewis base. Again, the adduct formation is essentially barrierless. After the adsorption, additional energy is needed to induce an intramolecular proton transfer from –NH_2 to one of the methyl groups in TMA. Evidently, the chemical bond of the proton in the NH_2 group is more stable than that in the OH group[54]. After completed proton transfer, the newly formed CH_4 desorbs and dimethylaluminium remains chemically bound to N with an energy gain of E_4=-83.4 kJ/mol. Given that the amine groups contain a second proton, a further reaction may be possible. The product of the calculated pathway R_2* for a second intramolecular proton transfer is shown in Figure 5 (E_5). The energy balance in that reaction is +190.5 kJ/mol relative to E_4, and thus this reaction is considered to be unfavorable. However, the reaction of multiple 4PD molecules with one TMA molecule appears possible (Figure S1). The further energy gains for a second and third elimination of CH_4 are -98.7 kJ/mol and -95.7 kJ/mol, favoring this scenario.
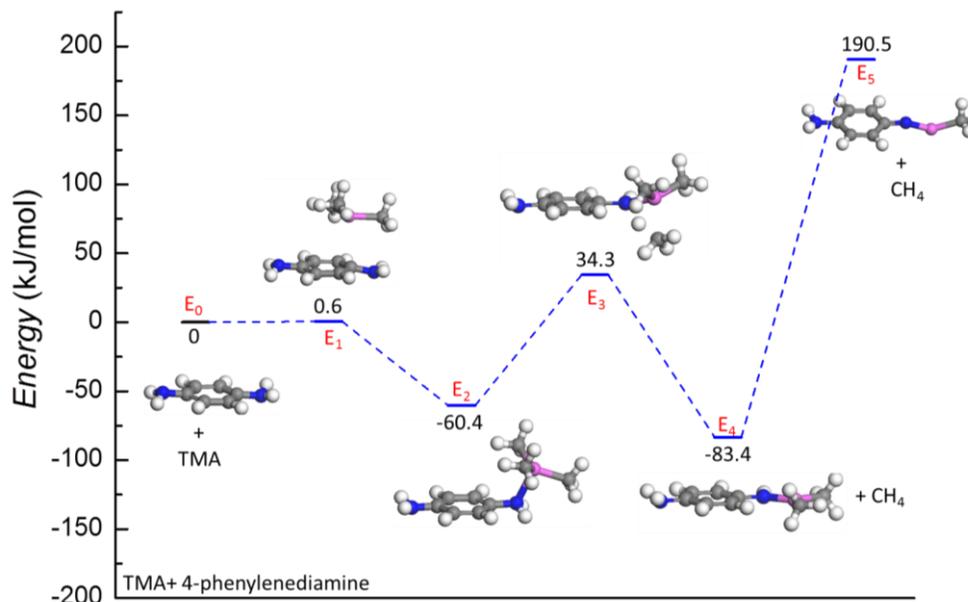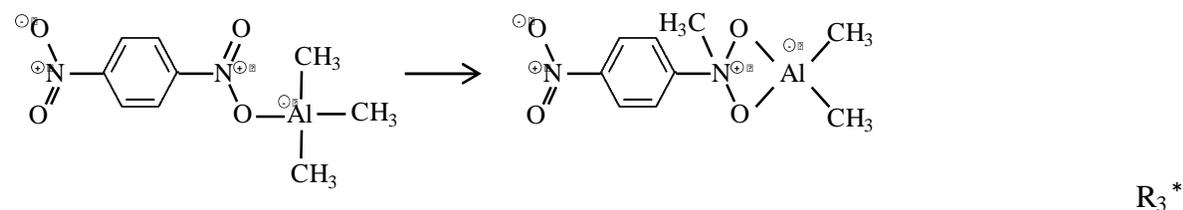
Figure 5. Calculated energy profile for the reaction pathways R_2 and R_2^* of TMA interacting with 4PD.

In contrast to the previously described molecules, 4DN does not contain acidic H for a possible reaction with the methyl groups of TMA. Nevertheless, a Lewis acid-base reaction may take place. A possible reaction scheme for TMA with 4DN is shown in R_3 below (showing just one of its resonance forms).


$$R_3$$
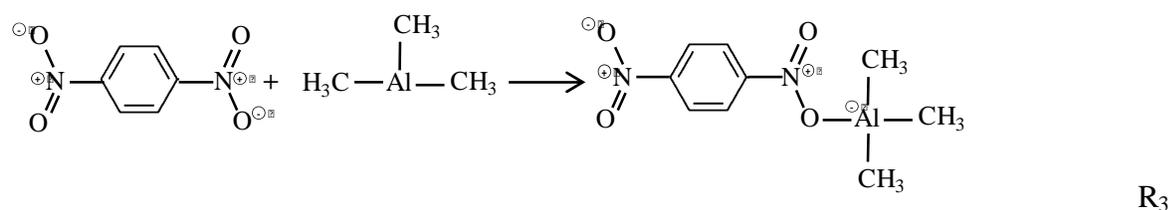
The charge distribution in the product suggests that intramolecular transfer of a methyl group may be possible, which should happen according to R_3^*:

$$R_3^*$$

The calculated energy profile for the reactions R_3 and R_3^* is shown in Figure 6. The interaction starts with a binding of TMA to a Lewis basic O atom, which is practically barrierless. However,

due to the lack of acidic H for reacting with the methyl group of TMA, $-CH_3$ may transfer to the electron-deficient N instead. In consequence, the liberated Al atom will bind with both O atoms to form a bridged link that is typical of aluminum oxide. This entire step requires substantial activation energy to overcome the barrier of E_3-E_2=84.6 kJ/mol. The final energy gain after this reaction is E_4=-161.4 kJ/mol relative to the isolated reactants. A possible reaction of multiple 4DN reacting with one TMA was also calculated and the further energy gains are -98.7 kJ/mol and -95.7 kJ/mol for each successive reaction (Figure S2).
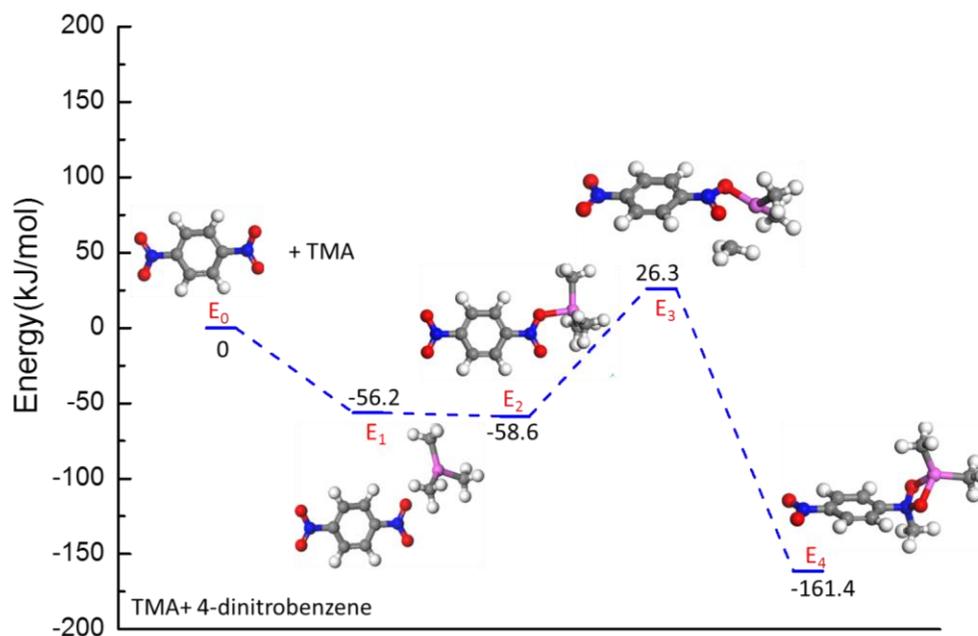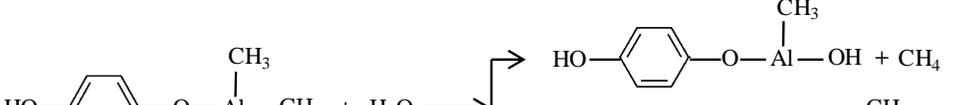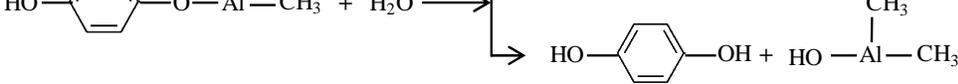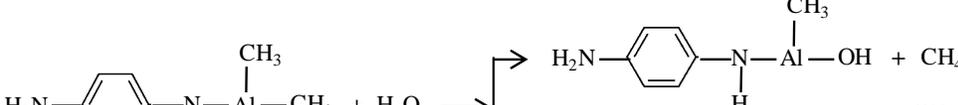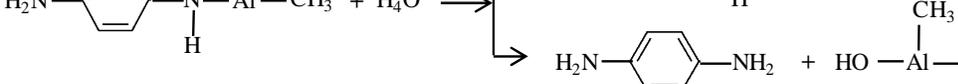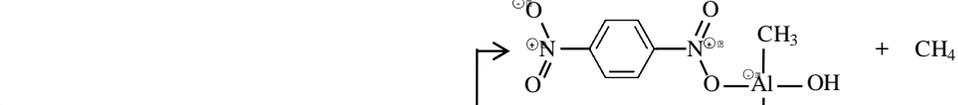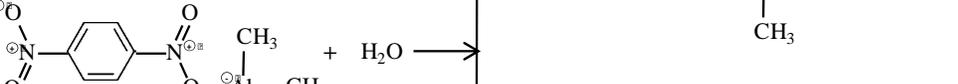

Figure 6. Calculated energy profile for the reactions R_3 and $R_3{}^*$ of TMA interacting with 4DN.

ALD/MLD grown thin films often change their chemical properties after exposure to air[6]. This most likely reason for this is hydrolysis of the chemical bonds with H_2O. Since our XPS experiments showed changes after exposure of the intermediates to air, we modeled possible reactions with H_2O of the products from R_1, R_2 and R_3. The resulting possible reaction schemes and energies are listed in Table 1 and Table S2. In each case, water can either eliminate CH_4 from the dimethylaluminium adduct (reactions labelled "a"), or hydrolyze the Al-O/Al-N adduct bond restoring the initial functionalized phenyl ring (reactions labelled "b"). Table 1 shows that the formation of CH_4 is the more exothermic reaction, consistently yielding -170 to -180 kJ/mol regardless of the involved functional group (R_{1a}, R_{2a}, R_{3a}, R_{3d}). Therefore, it is very likely that all remaining $Al-CH_3$ bonds will first be hydrolyzed by H_2O to convert the adduct to -$Al(OH)_2$ or -$Al(OH)_3$. We have not computed these hydroxide-based adducts, but expect that

their reactivity will follow a similar trend to that shown in Table 1. If so, when all Al-CH$_3$ has been hydrolyzed, the less exothermic hydrolysis of the adduct bond may then take place, restoring the amine group of 4PD (analogous to R$_{2b}$, -67.8 kJ/mol) or the nitro group of 4DN (analogous to R$_{3b}$, -116.1 kJ/mol). Unsurprisingly, cleavage of Al-O to restore 4HQ is less favourable (R$_{1b}$, -15.3 kJ/mol), so we suggest that the 4HQ-based adduct may remain intact even in the presence of H$_2$O.

Table 1. Selected reaction schemes and energy gains for possible reactions of MLD or VPI intermediates with humidity (H$_2$O); a more comprehensive list is in Table S2.

	ΔE (kJ/mol)
	-175.4 (R$_{1a}$)
	-15.3 (R$_{1b}$)
	-171.9 (R$_{2a}$)
	-67.8 (R$_{2b}$)
	-180.4 (R$_{3a}$)
	-116.1 (R$_{3b}$)

To summarize the calculated energetic profiles, the reaction starts in all three cases with molecular adsorption of TMA to specific sites of the functionalized benzene molecules. The calculated energies (Table 1) indicate that these adsorptions (Figure S3) are all exothermic and essentially barrierless at T=0 K and therefore likely to occur in all three cases. After the adsorption, kinetic barriers are observed for all three functional groups towards various reactions that dissociate the CH$_3$ groups of TMA. For –OH (4HQ) and –NH$_2$ (4PD) that contain acidic protons, thermal activation is needed for an intramolecular reaction between CH$_3$ and H, producing CH$_4$ and leaving behind strongly bound dimethylaluminium. For the NO$_2$-

functionalized molecule (4DN), since no acidic H is present, the alternative methyl group transfer to N also requires activation. The calculated activation energies for $-NH_2$ (94.7 kJ/mol) and NO_2 (84.6 kJ/mol) in Table 2 are much higher than for $-OH$ (32.5 kJ/mol). This means that the reaction with $-OH$ will proceed more rapidly. Consequently, TMA bound to 4PD or 4DN may not lose methyl groups to an appreciable extent under the given experimental conditions.

Table 2 shows that the activation energies (E_3-E_2) for reactions of TMA with $-NH_2$ and $-NO_2$ are also substantially higher than those for the reverse reaction (E_0-E_2), especially when entropy is considered (G_0-G_2). It is therefore more likely that the adducts of TMA with 4PD and 4DN will split again to form the pristine molecules, rather than the reaction proceeding according to R_2, R_2* or R_3*. Only in the case of 4HQ is the energy barrier for elimination of CH_4 (32.5 kJ/mol) lower than the TMA desorption energy (40.5 kJ/mol), indicating that elimination is likely until all CH_3 is consumed.

Table 2. Calculated adsorption energies and free energies, energy barriers and total energy gain for the potential reaction pathways of a single TMA with 4HQ, 4PD or 4DN, displayed in Figure 3, 5 and 6.

	Functional groups (molecules)	Molecular adsorption E_2-E_0 (kJ/mol)	Molecular adsorption $\Delta G = G_2 - G_0$ (kJ/mol) at 298.15 K	Energy barrier $E_a = E_3 - E_2$ (kJ/mol)	Reaction energy E_4 (kJ/mol)
Previous study	-OH (Al(OH)$_2$-OH)[50]	-58.8	-	50.2	-164
	-OH[51]	-109	-4.8	33.8	-67.5
	Al$_2$O$_3$-OH[52]	-67.5	-	86.8	-112.1
This work	–OH (4HQ)	-40.5	-1.8	32.5	-149.7
	–NH$_2$ (4PD)	-60.4	-16	94.7	-83.4
	–NO$_2$ (4DN)	-58.6	-20	84.6	-161.4

Consistent with this, in the XPS data for 4HQ no peak for $-CH_3$ is observed after TMA dosing (Figure 2a and Figure S4a). Also the position of the Al 2p peak is located at 75.6 eV, which is expected for Al_2O_3[48,55,56]. This suggests a quantitative formation of Al-O bonds after

dosing TMA to 4HQ. The finding that both C 1s and Al 2p showed only negligible changes upon exposure to air further supports this conclusion.

The core levels of the TMA-dosed 4PD sample show two particularities: (a) the shift of the N 1s core level towards higher BE indicates a formal increase of the oxidation state compared to the pristine pellet; (b) the unusually low BEs of 73.6 eV and 283.5 eV of the Al 2p and C 1s core levels, respectively, indicate a formal reduction of TMA where values of 74.8 and 284.8 eV are reported for condensed TMA films[47,48]. Similar chemical shifts of the C 1s and Al 2p core levels were observed previously for TMA adsorbed on a Si surface and are attributed to the interaction of TMA with dangling bonds on the Si substrate[57]. In our case this occurs most likely with the lone electron pairs of the amine groups.

In the 4PD-TMA Lewis adduct (E_2 in Figure 5), the N lone pair overlaps with the empty 3p orbital of Al, resulting in an electron density shift from N to Al. Consequently, N becomes more oxidized and Al more reduced. This tendency is obvious from the shift of the N 1s peak towards higher binding energies, if compared to 4PD. For the E_4 state, a shift of the N 1s core level towards lower binding energies would be expected[58–60]. Most likely the calculated high reaction barrier for the elimination of CH_4 from the 4PD adduct (R_2) favors the formation of the 4PD-TMA Lewis adduct rather than the E_4 product.

The interaction of TMA with 4DN must be different due to the lack of protons in NO_2. The C 1s at 283.5 eV (Figure S4c) and Al 2p at 73.8 eV (Figure 2b) are both in lower BE regions than observed from condensed TMA films[47,48], indicating an electron density shift from NO_2 towards TMA, similar to the 4PD sample. This strongly suggests the formation of a TMA-4DN Lewis adduct (E_2 state in Figure 6), as predicted by DFT. Ideally, the fingerprint of the N 1s at BE close to 406 eV would give deeper insight. However, its interpretation is challenging due to the complex superposition of XPS spectra resulting from X-ray[34,46] and TMA induced reduction of nitro to amine groups and a variety of possible shake-up processes[32,34,36,49]. An important observation is that the shift of the N 1s peak is reversed after exposure of the 4DN-TMA samples to air, indicating a cleavage of the bond between Al and 4DN. Moreover, the drop in intensity of CH_3 as well as the shift of the Al 2p level towards higher BEs points towards formation of alumina[48,55,56] resulting from the reaction with water, perhaps along the lines of computed reaction R_{3b} (Table 1). Thus, the scenario of methyl transfer to the NO_2 group is very unlikely.

Reactivity of TMA with hetero-substituted phenyl molecules

WILEY-VCH

The hetero-substituted phenyls 4-aminophenol (4AP), 4-nitrophenol (4NP) and 4-nitroaniline (4NA) were chosen to evaluate the preferential interaction of TMA in presence of two different functional groups. Figure 7 shows the C 1s, N 1s and Al 2p XPS spectra of 4AP, 4NP and 4NA in their native, TMA dosed and subsequently air (H_2O) exposed states.

The changes of the C 1s core levels of 4AP, 4NP and 4NA in Figure 7a are comparable to those previously observed for 4PD and 4DN in Figure 2a. The characteristic shoulder at lower binding energies appeared after TMA dosing and significantly decreased after further exposure to air. The Al 2p core levels in Figure 7b show comparable changes to the previously discussed cases of 4PD and 4DN. After exposure to TMA the Al 2p core level maxima of the 4AP and 4NP samples appear around 74 eV and after subsequent exposure to air, they shift by about 0.6-0.8 eV towards higher BE.

The evolution of N 1s core levels can likewise be described as a superposition of the previously discussed effects. Specifically, the single N 1s feature around 396.6 eV in 4AP shifted to around 400 eV when exposed to TMA and reversed almost entirely after exposure to air. The behavior is similar to 4PD, but the shift is less pronounced. For the 4NP, a new peak close to 400 eV evolved upon exposure to TMA, which shifted towards higher BE upon exposure to air. The original peak of the pristine sample remained unchanged. In the case of 4NA, the most significant difference to the other samples is the width of the peak at 406 eV. Once exposed to TMA its intensity reduced and the peak shifted substantially towards lower BEs. After subsequent exposure to air, its intensity further reduced and the peak shifted back to some extent towards higher BEs.
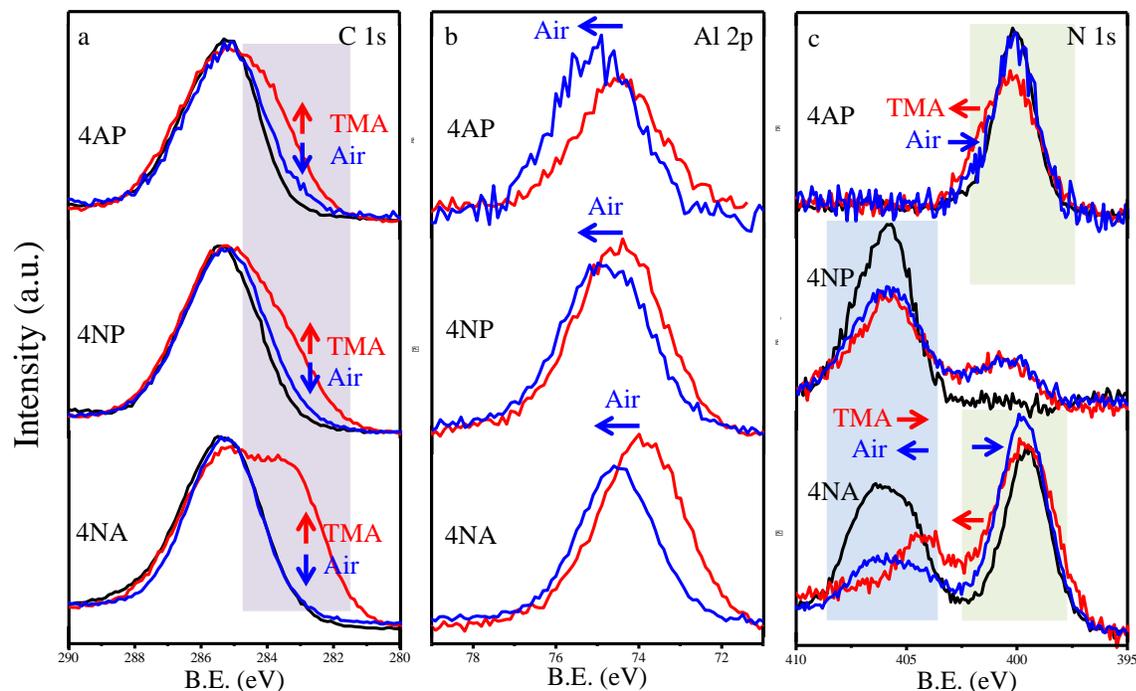
Figure 7. (a) C 1s, (b) Al 2p and (c) N 1s XPS spectra of 4-aminophenol (4AP), 4-nitrophenol (4NP) and 4-nitrobenzene (4NA) in the native (black curve), TMA dosed (red curve) and air exposed (blue curve) states. Arrows in the figures indicate the changes of the peaks in the marked zone upon treatment with TMA and subsequently with air.

Out of those experimental observations, following conclusions can be drawn. (i) Whenever hydroxyl groups are present, TMA will irreversibly react with them. This can be derived from the observation that after exposure to TMA the CH_3 contribution to the XPS spectra in the 4AP and 4NP samples was roughly half of that in the respective 4DN, 4PD and 4NA samples (see Supplementary Figure S4). (ii) The reversible formation of TMA-4PD or TMA-4DN adducts is expected, considering that the changes in the C 1s, N 1s and Al 2p core levels are analogous for hetero-substituted and homo-substituted phenyls (Table S1).

An interesting observation is that the color of 4-nitroaniline (4NA) changed from its original yellow to pure red during dosing with TMA in an *ex situ* experiment, where 4NA was dissolved in ethanol and drop casted onto ultrasound cleaned glass slides and dried. The glass slide was then placed into the reactor of a Savannah 100 (Cambridge Nanotech Inc.) and infiltrated with TMA at 80 °C. However, after exposing the sample to air, the red color turns back to yellow within seconds. This is a clear evidence of a reversible interaction between TMA

and 4NA. Most likely, the electronic state of the 4NA becomes disturbed upon binding of TMA, which seriously affects the optical absorption of the molecule.

Molecular interactions in an MLD type of process on a TiO_2 surface
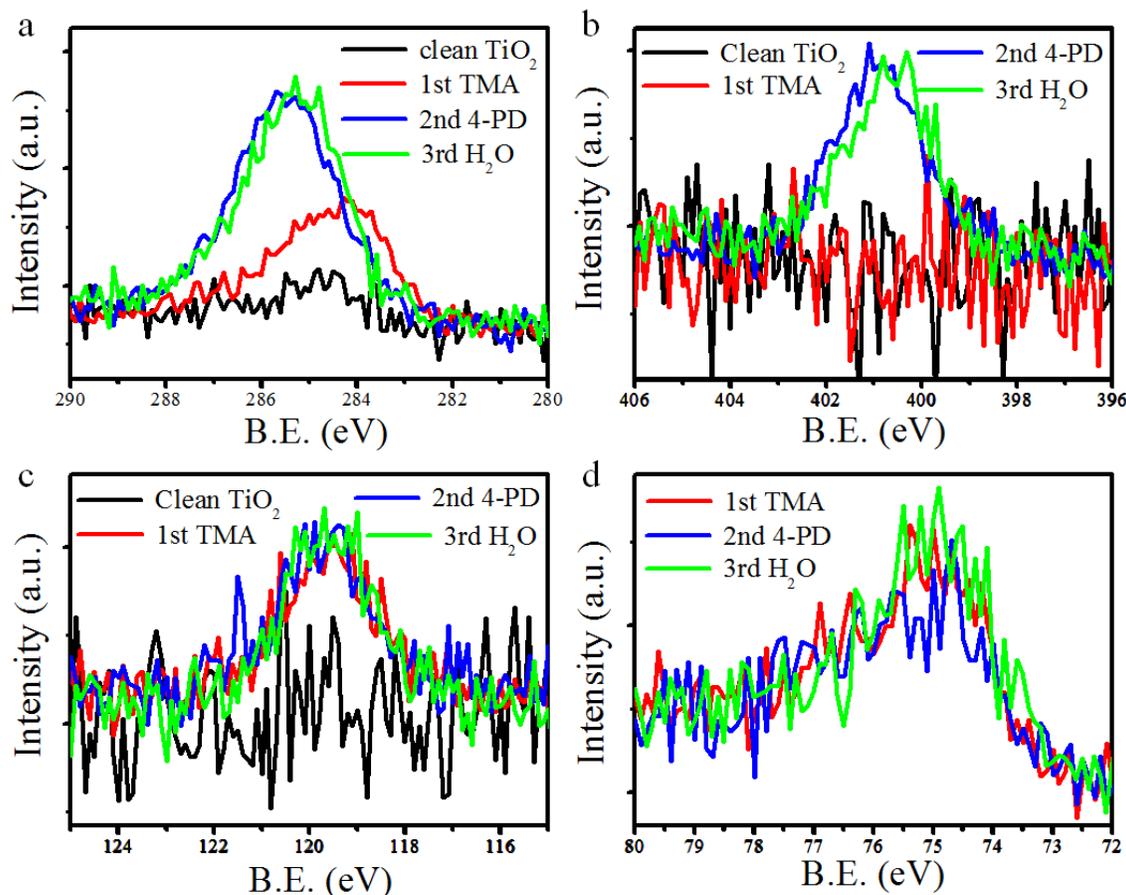
Figure 8. (a) C 1s, (b) N 1s, (c) Al 2s and (d) Al 2p XPS spectra of TiO_2, after 4-phenylenediamine dosing, after further TMA dosing and finally exposure to H_2O.

As MLD processes are normally performed on a solid substrate, in a further experiment the interactions of TMA with 4PD were investigated on a clean rutile (110) TiO_2 surface, in analogy to an MLD process. Here, TMA was first dosed to the clean TiO_2 surface and subsequently 4PD was introduced to interact with the adsorbed TMA. After TMA dosing, the C 1s, Al 2s and 2p peaks evolve in the XPS spectra shown in Figure 8. Upon dosing of 4PD, the position of the C 1s peak in Figure 8a changes owing to the contribution from the carbons from the phenyl ring in 4PD. Upon exposure to H_2O, the N 1s peak from $–NH_2$ shifts towards lower binding energies to a small amount, which indicates a change of the electronic state of the N. Figure 5 shows two energetically favored products (E_2 and E_4), both of which will react further

WILEY-VCH

in presence of water under hydrolysis of the bond between Al and N. Considering the shift of the N 1s peak to lower BEs, the reaction product after TMA dosing can only be the E_2 state, where the N in the TMA-4PD adduct is in a lower oxidation state compared to pristine 4PD. Therefore, the reversible adduct formation between amine-containing molecules and TMA precursors is expected to be valid for both MLD growth and infiltration processes. Although cleavage of the Al-N adduct bond implies that the 4PD would desorb from the surface after hydrolysis, the spectrum in Figure 8b clearly shows a presence of N after exposure to air. A very likely scenario is that the resulting $Al(OH)_3$ and 4PD remain bound through hydrogen bonds.

Conclusions

Understanding the reactivity between functional organic molecules and organometallic precursors is important for both the molecular layer deposition (MLD) and vapor phase infiltration processes. In this work, we studied the reactivity between some typical organic functional groups and trimethylaluminium (TMA) in a concerted experimental and theoretical approach. Six organic molecules with various combinations of hydroxyl, amino and nitro functionalities were chosen for the investigation. The experimental and theoretical results are in good agreement and yield the following picture. (i) Reactions between TMA and the functional groups are exothermic, but the dissociation of methyl groups from TMA requires an activation barrier to be overcome. It is evident that the reaction sequence for TMA with $-NH_2$ or $-NO_2$ functional groups is considerably slower than that with $-OH$. (ii) Thermal energy is also needed for the competing reverse reaction of desorption of unreacted TMA. (iii) In a reaction with water, producing methane is thermodynamically more favored than cleaving the adduct between Al and the functional group.

Each of the functional groups shows a different level of stability upon reaction with TMA under these process conditions. Our concerted XPS and DFT investigations show that in presence of $-OH$, Al will tightly bind to oxygen, eliminating H and CH_3. The reaction is irreversible and quantitative until all methyl groups are consumed. In the case of $-NH_2$, TMA will reversibly adsorb to the nitrogen site. Upon reaction with water, $Al(OH)_3$ will form and then the Al-N bond will be cleaved. Intermolecular interaction in the form of hydrogen bonds between $Al(OH)_3$ and the NH_2 group is likely to remain. Finally, in the case of $-NO_2$, the XPS spectra indicate that TMA will reversibly adsorb to only one of the oxygen atoms and, like $-NH_2$, desorb as $Al(OH)_3$ upon reaction with water.

The results can be largely correlated to some previous reports. The MLD process using TMA and 4-hydroquinone was successfully performed and studied at low temperatures[61–63]. However, only one publication described the MLD process involving TMA and 4-phenylenediamine, which works at 400 ℃. The resulting film is unstable and decomposes upon contact with humidity[64]. Furthermore, for ALD processes it is known that aluminum oxide is much easier grown than aluminum nitride[65]. The nitride processes typically require much higher processing temperatures with NH_3 or alternatively need assistance of nitrogen plasma[66–68]. Those results are in good agreement with our observations that higher energy barriers need to be overcome for obtaining an Al-N binding, which still may not be stable upon contact with humidity. Concerning nitro groups, no corresponding MLD processes with TMA have been reported so far. However, nitro groups have been witnessed to enable adsorption of TMA to inert substrates and thus nucleation of alumina. This was achieved by first dosing NO_2 gas onto carbon nanotubes or graphene, or grafting of carbon nanotubes with 4-nitroaniline. TMA adsorbed to those molecules and subsequently allowed a growth of Al_2O_3[69–72]. Those experiments verify that at least *in-situ* an interaction of nitro groups and TMA occurs, indicating at least a weak interaction between TMA and nitro groups as observed in the present work.

The calculations further predict that TMA may react with amine or nitro groups via methyl-transfer to give stable products, but only if the substantial activation barrier is overcome. This indicates the possibility of fabricating novel Al-N-based or Al-O-N-based hybrid materials if sufficient thermal energy is supplied during the reaction.

The results presented here are only a first step towards in-depth understanding of the vast variety of possibilities to direct the formation of hybrid materials by choice of the functional groups in the organic or polymeric substrate. However, the presented insight may already prove helpful for the design of processes by MLD or modification of soft materials by vapor phase infiltration.

Supporting Information
Supporting Information is available at the Wiley Online Library or from the author.

WILEY-VCH

Received: ((will be filled in by the editorial staff))
Revised: ((will be filled in by the editorial staff))
Published online: ((will be filled in by the editorial staff))

Reference

[1]   C. Sanchez, B. Julián, P. Belleville, M. Popall, *J. Mater. Chem.* **2005**, *15*, 3559.

[2]   S. V Dorozhkin, *Biomatter* **2011**, *1*, 3.

[3]   L. De Bartolo, A. Leindlein, D. Hofmann, A. Bader, A. de Grey, E. Curcio, E. Drioli, *Chem. Eng. Process. Process Intensif.* **2012**, *51*, 79.

[4]   E. K. Hendow, P. Guhmann, B. Wright, P. Sofokleous, N. Parmar, R. M. Day, *Fibrogenesis Tissue Repair* **2016**, *9*, 3.

[5]   S. M. George, *Chem. Rev.* **2010**, *110*, 111.

[6]   P. Sundberg, M. Karppinen, *Beilstein J. Nanotechnol.* **2014**, *5*, 1104.

[7]   B. H. Lee, B. Yoon, A. I. Abdulagatov, R. a. Hall, S. M. George, *Adv. Funct. Mater.* **2013**, *23*, 532.

[8]   K. Gregorczyk, M. Knez, *Prog. Mater. Sci.* **2016**, *75*, 1.

[9]   S. Cho, G. Han, K. Kim, M. M. Sung, *Angew. Chem. Int. Ed.* **2011**, *50*, 2742.

[10]   J. Liu, B. Yoon, E. Kuhlmann, M. Tian, J. Zhu, S. M. George, Y. Lee, R. Yang, *Nano Lett.* **2013**, *13*, 5594.

[11]   B. Yoon, B. H. Lee, S. M. George, *J. Phys. Chem. C* **2012**, *116*, 24784.

[12]   Q. Peng, B. Gong, R. M. Vangundy, G. N. Parsons, *Chem. Mater.* **2009**, *21*, 820.

[13]   A. Sood, P. Sundberg, M. Karppinen, *Dalton Trans.* **2013**, *42*, 3869.

[14]   B. Yoon, D. Seghete, A. S. Cavanagh, S. M. George, *Chem. Mater.* **2009**, *21*, 5365.

[15]   S. Jen, S. M. George, *ACS Appl. Mater. Interfaces* **2013**, *5*, 1165.

[16]   B. H. Lee, B. Yoon, V. R. Anderson, S. M. George, *J. Phys. Chem. C* **2012**, *116*, 3250.

[17]   A. Sood, P. Sundberg, J. Malm, M. Karppinen, *Appl. Surf. Sci.* **2011**, *257*, 6435.

[18]   S. Ishchuk, D. H. Taffa, O. Hazut, N. Kaynan, R. Yerushalmi, *ACS Nano* **2012**, 7263.

[19]   D. Sarkar, D. H. Taffa, S. Ishchuk, O. Hazut, H. Cohen, G. Toker, M. Asscher, R. Yerushalmi, *Chem. Commun.* **2014**, *50*, 9176.

[20]   B. H. Lee, V. R. Anderson, S. M. George, *Chem. Vap. Depos.* **2013**, *19*, 204.

[21]   B. H. Lee, V. R. Anderson, S. M. George, *ACS Appl. Mater. Interfaces* **2014**, *6*, 16880.

[22]   L. Zhang, A. J. Patil, L. Li, A. Schierhorn, S. Mann, U. Gösele, M. Knez, *Angew. Chem. Int. Ed.* **2009**, *48*, 4982.

[23]   S.-M. Lee, V. Ischenko, E. Pippel, A. Masic, O. Moutanabbir, P. Fratzl, M. Knez, *Adv.*

WILEY-VCH

Funct. Mater. **2011**, *21*, 3047.

[24] S.-M. Lee, E. Pippel, U. Gösele, C. Dresbach, Y. Qin, C. V. Chandran, T. Bräuniger, G. Hause, M. Knez, *Science* **2009**, *324*, 488.

[25] S.-M. Lee, E. Pippel, M. Knez, *Chemphyschem* **2011**, *12*, 791.

[26] S.-M. Lee, E. Pippel, O. Moutanabbir, I. Gunkel, T. Thurn-Albrecht, M. Knez, *ACS Appl. Mater. Interfaces* **2010**, *2*, 2436.

[27] K. E. Gregorczyk, D. F. Pickup, M. G. Sanz, I. A. Irakulis, C. Rogero, M. Knez, *Chem. Mater.* **2015**, *27*, 181.

[28] S. D. Elliott, G. Dey, Y. Maimaiti, H. Ablat, E. A. Filatova, G. N. Fomengia, *Adv. Mater.* **2016**, *28*, 5367.

[29] C. Draxl, D. Nabok, K. Hannewald, *Acc. Chem. Res.* **2014**, *47*, 3225.

[30] A. J. Karttunen, T. Tynell, M. Karppinen, *J. Phys. Chem. C* **2015**, *119*, 13105.

[31] P. W. Loscutoff, H. Zhou, S. B. Clendenning, S. F. Bent, *ACS Nano* **2010**, *4*, 331.

[32] A. Katrib, N. R. El-Rayyes, *Chem. Phys.* **1981**, *59*, 443.

[33] S. X. Huang, D. A. Fischer, J. L. Gland, *J. Phys. Chem.* **1996**, 10223.

[34] K. Roodenko, M. Gensch, J. Rappich, K. Hinrichs, N. Esser, R. Hunger, D. Elektronen-synchrotron, H. Berlin, *J. Phys. Chem. B* **2007**, *111*, 7541.

[35] M. S. Banna, *Chem. Phys.* **1980**, *45*, 383.

[36] H. Ågren, B. O. Roos, P. S. Bagus, U. Gelius, P. Malmquist, S. Svensson, R. Maripuu, K. Siegbahn, *J. Chem. Phys.* **1982**, *77*, 3893.

[37] H. -J. Freund, A. R. Slaughter, S. M. Ballina, M. S. Banna, R. W. Bigelow, B. Dick, J. Lex, H. M. Deger, *J. Chem. Phys.* **1984**, *81*, 2535.

[38] B. Folkesson, P. Sundberg, *Spectrosc. Lett.* **1987**, *20*, 193.

[39] T. Ohta, M. Yamada, H. Kuroda, *Bull. Chem. Soc. Jpn.* **1974**, *47*, 1158.

[40] J. L. Solomon, R. J. Madix, *Surf. Sci.* **1991**, *255*, 12.

[41] D. Sholl, J. A. Steckel, *Density Functional Theory: A Practical Introduction*, John Wiley & Sons, Inc., New Jersey, **2002**.

[42] R. Ahlrichs, *Phys. Chem. Chem. Phys.* **2004**, *6*, 5119.

[43] F. Weigend, *Phys. Chem. Chem. Phys.* **2006**, *8*, 1057.

[44] F. Furche, R. Ahlrichs, C. Hättig, W. Klopper, M. Sierka, F. Weigend, *Wiley Interdiscip. Rev. Comput. Mol. Sci.* **2014**, *4*, 91.

[45] C. Peng, P. Y. Ayala, H. B. Schlegel, M. J. Frisch, *J. Comput. Chem.* **1996**, *17*, 49.

[46] J. H. Moon, K. Kim, T. Kang, B. Kim, H. Kang, J. W. Park, *Langmuir* **1998**, *14*, 5673.

[47] D. Lubben, T. Motooka, J. E. Greene, J. F. Wendelken, J.-E. Sundgren, W. R. Salaneck, *Mater. Res. Soc. Symponisum Proc.* **1988**, *101*, 151.

[48] D. R. Strongin, J. F. Moore, M. W. Ruckman, *Appl. Phys. Lett.* **1992**, *61*, 729.

[49] G. Distefano, M. Guerra, F. P. Colonna, D. Jones, *Chem. Phys.* **1982**, *72*, 267.

WILEY-VCH

[50] Y. Widjaja, C. B. Musgrave, *Appl. Phys. Lett.* **2002**, *80*, 3304.

[51] T. Weckman, K. Laasonen, *Phys. Chem. Chem. Phys.* **2015**, *17*, 17322.

[52] S. D. Elliott, J. C. Greer, *J. Mater. Chem.* **2004**, *14*, 3246.

[53] M. Shirazi, S. D. Elliott, *Nanoscale* **2015**, *7*, 6311.

[54] C. A. Murray, S. D. Elliott, D. Hausmann, J. Henri, A. LaVoie, *ACS Appl. Mater. Interfaces* **2014**, *6*, 10534.

[55] E. Ozensoy, C. H. F. Peden, J. Szanyi, *J. Phys. Chem. B* **2005**, *109*, 15977.

[56] J. A. Taylor, *J. Vac. Sci. Technol.* **1982**, *20*, 751.

[57] W. R. Salaneck, R. Bergman, J. E. Sundgren, A. Rockett, T. Motooka, J. E. Greene, *Surf. Sci.* **1988**, *198*, 461.

[58] L. Rosenberger, R. Baird, E. McCullen, G. Auner, G. Shreve, *Surf. Interface Anal.* **2008**, *40*, 1254.

[59] R. Dalmau, R. Collazo, S. Mita, Z. Sitar, *J. Electron. Mater.* **2007**, *36*, 414.

[60] K. Artyushkova, B. Kiefer, B. Halevi, a Knop-Gericke, R. Schlogl, P. Atanassov, *Chem. Commun.* **2013**, *49*, 2539.

[61] O. Nilsen, K. B. Klepper, H. Ø. Nielsen, H. Fjellvåg, *ECS Trans.* **2008**, *16*, 3.

[62] O. Nilsen, H. Fjellvåg, *J. Therm. Anal. Calorim.* **2011**, *105*, 33.

[63] T. Tynell, I. Terasaki, H. Yamauchi, M. Karppinen, *J. Mater. Chem. A* **2013**, *1*, 13619.

[64] W. Zhou, J. Leem, I. Park, Y. Li, Z. Jin, Y.-S. Min, *J. Mater. Chem.* **2012**, *22*, 23935.

[65] R. L. Puurunen, *J. Appl. Phys.* **2005**, *97*, 121301.

[66] X. Liu, S. Ramanathan, E. Lee, T. E. Seidel, *Mater. Res. Soc. symponisum Proc.* **2004**, *811*, D1.9.1.

[67] S. Goerke, M. Ziegler, A. Ihring, J. Dellith, A. Undisz, M. Diegel, S. Anders, U. Huebner, M. Rettenmayr, H.-G. Meyer, *Appl. Surf. Sci.* **2015**, *338*, 35.

[68] M. Bosund, T. Sajavaara, M. Laitinen, T. Huhtio, M. Putkonen, V.-M. Airaksinen, H. Lipsanen, *Appl. Surf. Sci.* **2011**, *257*, 7827.

[69] D. B. Farmer, R. G. Gordon, *Electrochem. Solid-State Lett.* **2005**, *8*, G89.

[70] A. S. Cavanagh, C. a Wilson, A. W. Weimer, S. M. George, *Nanotechnology* **2009**, *20*, 255602.

[71] D. B. Farmer, R. G. Gordon, *Nano Lett.* **2006**, *6*, 699.

[72] X. Wang, S. M. Tabakman, H. Dai, *J. Am. Chem. Soc.* **2008**, *130*, 8152.